Modification of silicone elastomers with Bioglass 45S5® increases in ovo tissue biointegration

Cohrs, Nicholas H ; Schulz-Schönhagen, Konstantin ; Mohn, Dirk ; Wolint, Petra ; Meier Bürgisser, Gabriella ; Stark, Wendelin J ; Buschmann, Johanna

Abstract: Silicone is an important material family used for various medical implants. It is biocompatible, but its bioinertness prevents cell attachment, and thus tissue biointegration of silicone implants. This often results in constrictive fibrosis and implant failure. Bioglass 45S5® (BG) could be a suitable material to alter the properties of silicone, render it bioactive and improve tissue integration. Therefore, BG micro- or nanoparticles were blended into medical-grade silicone and 2D as well as 3D structures of the resulting composites were analyzed in ovo by a chick chorioallantoic membrane (CAM) assay. The biomechanical properties of the composites were measured and the bioactivity of the composites was verified in simulated body fluid. The bioactivity of BG-containing composites was confirmed visually by the formation of hydroxyapatite through scanning electron microscopy as well as by infrared spectroscopy. BG stiffens as prepared non-porous composites by 13% and 36% for micro- and nanocomposites respectively. In particular, after implantation for 7 days, the Young's modulus had increased significantly from 1.20 ± 0.01 to 1.57 ± 0.03 MPa for microcomposites and 1.44 ± 0.03 to 1.69 ± 0.29 MPa to for nanocpmosites. Still, the materials remain highly elastic and are comparably soft. The incorporation of BG into silicone overcame the bioinertness of the pure polymer. Although the overall tissue integration was weak, it was significantly improved for BG-containing porous silicones (+72% for microcomposites) and even further enhanced for composites containing nanoparticles (+94%). These findings make BG a suitable material to improve silicone implant properties. © 2018 Wiley Periodicals, Inc. J Biomed Mater Res B Part B: Appl Biomater, 2018.

DOI: https://doi.org/10.1002/jbm.b.34211

Modification of silicone elastomers with Bioglass 45S5® increases *in ovo* tissue biointegration

Nicholas H. Cohrs[a], Konstantin Schulz-Schönhagen[a], Dirk Mohn[a,b], Petra Wolint[c], Gabriella Meier Bürgisser[c], Wendelin J. Stark[a] and Johanna Buschmann[c,*]

a. Institute for Chemical- and Bioengineering, Department of Chemistry and Applied Biosciences, ETH Zürich, Zürich, Switzerland.
b. Clinic of Preventive Dentistry, Periodontology and Cariology, University of Zürich, Center of Dental Medicine, Zürich, Switzerland.
c. Division of Plastic and Hand Surgery, University Hospital Zürich, ZKF, Zürich, Switzerland.

* corresponding author: Dr Johanna Buschmann, University Hospital Zürich, Division of Plastic and Hand Surgery, E LAB 27, Sternwartstrasse 14, 8091 Zürich, Switzerland. Phone: +41 44 255 98 95, Fax +41 44 255 50 47.

Abstract

Silicone is an important material family used for various medical implants. It is biocompatible, but its bioinertness prevents cell attachment and, thus, tissue biointegration of silicone implants. This often results in constrictive fibrosis and implant failure. Bioglass 45S5® (BG) could be a suitable material to alter the properties of silicone, render it bioactive and improve tissue integration. Therefore, BG micro- or nanoparticles were blended into medical-grade silicone and 2D as well as 3D structures of the resulting composites were analyzed *in oo* by a chick chorioallantoic membrane (CAM) assay. The biomechanical properties of the composites were measured and the bioactivity of the composites was verified in simulated body fluid. The bioactivity of BG-containing composites was confirmed visually by the formation of hydroxyapatite through scanning electron microscopy as well as by infrared spectroscopy. BG stiffens as prepared non-porous composites by 13% and 36% for micro- and nanocomposites respectively. In particular, after implantation for 7 days, the Young's modulus had increased significantly from 1.20 ± 0.01 MPa to 1.57 ± 0.03 MPa for microcomposites and 1.44 ± 0.03 MPa to 1.69 ± 0.29 MPa to for nanocpmosites.. Still, the materials remain highly elastic and are comparably soft. The incorporation of BG into silicone overcame the bioinertness of the pure polymer. Although the overall tissue integration was weak, it was significantly improved for BG-containing porous silicones (+ 72 % for microcomposites) and even further enhanced for composites containing nanoparticles(+ 94 %). These findings make BG a suitable material to improve silicone implant properties.

Keywords: Silicone implants, tissue biointegration, *in ovo*, CAM assay, bioactive glass

1. Introduction

Silicone elastomers are a frequently used material family for the production of medical devices and used in implants, such as pacemakers, breast implants and artificial blood pumps.[1-4] The long-term stability of these implants inside the human body is a crucial factor for their success. Adverse events during the lifetime of implants, such as infections or fibrotic reactions, are severe clinical problems and affect the quality of life of patients significantly.[5-6] Silicones were tested for thrombosis, coagulation, platelet activation, leukocyte activation, haemolysis, and complement activation in a wide range of possible applications and did not show any adverse effects.[7]

However, clinicians from different fields, such as cardiac or plastic surgery, are frequently forced to exchange failing implants manufactured of silicone elastomers. The material's bioinertness can be the cause of this failure as it does not allow sufficient cell attachment and therefore impedes tissue adhesion and implant anchorage.[8] This is a particular problem for silicone breast implants, where the lack of cell attachment of the breast tissue to the silicone material and continuous micro-movement at the implant(silicone)-tissue interface frequently triggers constrictive fibrosis.[9] Similarly, percutaneous implants, such as ventricular assist device drivelines or catheters, are frequently made of silicone. As the skin cannot adhere to the silicone, these devices continuously disrupt the skin's protective barrier against pathogens.[10] As a consequence, the skin suffers from continued micro-trauma, which (i) compromises the integrity of the silicone-skin interface, (ii) gives an entry point for germs and (iii) causes chronical inflammatory reactions of the body.[6, 11-12] Biointegration of the driveline into the skin by wound healing around the device, formation of an interface between the material and tissue, and prevention of pathogen invasion would be a suitable approach to close the protective barrier and stabilize the implant.[10] These clinical examples

demonstrate the desire of clinicians and patients for a long-term stable silicone-tissue connection. Continuous trauma, mechanical irritation, infections and fibrous encapsulation would be reduced.

A suitable material to modify silicone material in order to address the aforementioned problems is bioactive glass. This inorganic material can provide silicone with the desired bio-integrative properties. Previously, we have shown that the incorporation of bioactive glass particles into medical-grade silicone improves the cell proliferation of primary human dermal fibroblasts on medical-grade silicone.[12] Bioactive glass is an amorphous material, which is available in various compositions.[13] Its best-known form is Bioglass 45S5® (BG), invented by Larry Hench in 1971 with a composition of 45 wt% SiO_2, 24.5 wt% Na_2O, 24.5 wt% CaO and 6 wt% P_2O_5.[13-15] While implanted, BG leaches ions into the body fluids and has a stimulatory effect on angiogenesis and wound healing.[16-18] Additionally, it possesses antibacterial properties, which renders it advantageous in contact with soft tissue.[16, 19] Finally, after transformation to hydroxyapatite (HAp), it enables the bonding to collagen. [20]

The study presented here continues on from our report about BG-silicone composites, which could not show improved tissue adhesion at first but only bioactivity and improved cytocompatibility on smooth samples.[12] Here, we report an *in ovo* evaluation of non-porous and porous BG-silicone composites using a chick chorioallantoic membrane (CAM) assay. We describe the manufacturing process of porous BG-silicone composites, incorporating either micron- or nanosized BG, an *in vitro* study in simulated body fluid (SBF) and the influence of the particles and porosity on the mechanical properties of silicone. The *in ovo* study gives additional information regarding living tissue biointegration of BG-containing silicone foams and justifies the use of BG in medical-grade silicone elastomers.

2. Materials and Methods

2.1. Manufacturing of Bioglass 45S5® silicone composites

Bioglass 45S5® microparticles (mBG) with a supplier-specified mean particle size of 4.1 μm (d50) were purchased from Schott (mBG, bioactive glass 45S5®, SCHOTT, Landshut, Germany). Bioglass 45S5® nanoparticles (nBG) were manufactured by means of flame spray synthesis as described earlier by Brunner *et al*.[21] Briefly, the corresponding amounts of silicone-, sodium-, calcium- and phosphorous precursors were mixed and diluted with tetrahydrofuran (inhibitor-free, Sigma-Aldrich, Buchs, Switzerland) at a volumetric ratio of 2:1. The mixture was dispersed in oxygen and ignited in a methane/oxygen flame. The nanoparticles were collected on a filter and sieved.

Six types of materials were manufactured: pure silicone elastomer and silicone elastomer containing 5 wt% mBG or 5 wt% nBG. All three compositions were manufactured in nonporous as well as in porous form. A medical-grade 2 component platinum addition cure silicone elastomer (silicone, Silicone Elastomer A-103, Factor II Inc., Lakeside AZ, USA) was purchased. The corresponding amount of BG was mixed with component A of the silicone in a dual-axis centrifuge mixer (Speed Mixer DAC 150 FVZ, Hauschild Engineering, Hamm, Germany) at 3500 rounds per minute (rpm) for 2 minutes. Subsequently, ammonium bicarbonate (NH_4HCO_3, BioUltra, $\geq$ 99.5%, Fluka Analytical, Steinheim, Germany) was added as a porogen at a concentration of 20 wt% with respect to the mass of silicone component A and mixed for 2 min at 3500 rpm, subsequently. The corresponding amount of silicone component B was added and mixed for 1 min at 3500 rpm. The uncured mixture was transferred into a syringe, degassed in a desiccator at 8 mbar for at least 10 min and transferred to a clean Teflon cylinder (diameter = 30 mm,

depth = 40 mm). The silicone was cured in an oven at 200 °C for 2 hours and the porogen evaporated simultaneously.

Additionally, nonporous samples of the same compositions were manufactured. The materials were prepared as described earlier.[12] Briefly, corresponding amounts of silicone component A and BG were mixed in a Speed Mixer and degassed for several times. Subsequently, silicone component B was added, mixed, transferred to a syringe and degassed to 8 mbar for at least 10 mins. Uncured mixtures were poured into a Teflon form, degassed until all entrapped air bubbles were removed and cured at RT overnight to yield a smooth surface. Afterwards, the composites were post-cured for 24 hours at 100 °C.

Thermogravimetric analysis (TG, Linseis TG/STA-PT1600, Selb, Germany) was used to investigate the manufacturing process and assure complete removal of the porogen material. Approximately 25 mg samples were heated at a rate of 10 °C min^{-1} from RT to 200 °C and kept for 2 hours.

2.2. Characterization of the materials

2.2.1. Particles. nBG, mBG and porogen particles were analyzed by scanning electron microscopy (SEM, FEI NovaNanoSEM450, FEI, The Netherlands) after being sputtered with a 5 nm layer of platinum. A particle size distribution (PSD) of ammonium bicarbonate was measured by taking the average diameter of all 298 particles present in a randomly chosen area of the SEM sample holder. The particle diameter was calculated by fitting the particles' appearance in the SEM images with an ellipse and taking the average of the major axis and minor axis of each particle as the individual particle diameter.

2.2.2. *In vitro* analysis using simulated body fluid. *In vitro* bioactivities of porous samples were determined using a SBF assay, prepared according to Kokubo and Takadama with a pH of 7.4.[22] Chemicals with a purity of Ph. Eur. were used for the preparation of SBF. Samples of porous BG-

silicone composites were cut with a scalpel yielding cubical shapes of approximately 5 mm x 5 mm x 5 mm ($n = 5$). Samples were washed in ethanol (EtOH, purists. p.a., Sigma Aldrich), subsequently dried in vacuum overnight at RT and weighted ($M_{0,\,dry}$). Samples (approx. 50 mg) were immersed in 5 mL of fresh SBF and incubated in a water bath at 37 °C for 4 weeks. SBF was exchanged once a week. After 4 weeks, samples were gently dried on paper and weighted ($M_{t,\,wet}$). Subsequently, samples were dried in vacuum for 1 week and weighted ($M_{t,\,dry}$). Weight loss (*%WL*) and water uptake (*%WA*) were calculated with the following formulas:[23]

$$\%WL = \left(\frac{M_{0,dry} - M_{t,dry}}{M_{0,dry}}\right) \times 100$$

$$\%WA = \left(\frac{M_{t,wet} - M_{t,dry}}{M_{\mathrm{t},dry}}\right) \times 100.$$

As prepared and immersed samples were analysed by SEM. Samples were frozen in liquid nitrogen and broken for cross-sectional observations.[24] Broken samples were mounted on carbon tape on the sample holder and sputtered with a 5 nm platinum layer. *In vitro* bioactivity of samples was determined by the formation of hydroxyapatite (HAp), which was identified visually by SEM.

HAp formation on the composites after immersion in SBF was analyzed using Fourier-transformed infrared spectroscopy (Bruker Tensor 27 FT-IR Spectrometer, Etlingen, Germany). Samples were burned in an oven at 700°C for 2 hours. The particulate samples were ground at 5 wt% in KBr. The IR spectra of the composites after immersion in SBF were measured versus a background of the respective composite before immersion in SBF. The spectra were collected in a frequency range of 500-1300 cm^{-1} and accumulating 100 scans. The spectra were not base-line corrected and not nomralised.

2.3. Physical properties of the composites

Porosities of foams were measured by cutting samples to sheets with a thickness of approximately 10 mm. Circular pieces of foams with a diameter of 12 mm were punched

from the sheets.The thickness of each sample was measured with calipers. Subsequently, samples were weighted on a balance. Porosities were calculated by comparing the densities of porous composites with the calculated densities of the non-porous samples ($n = 4$).

Stiffness of non-porous composites was measured before and after implantation in chicken embryos to evaluate the change of stiffness under *in ovo* conditions (see below) using ASTM Norm D412-16. Implanted samples were washed with phosphate buffered saline solution (PBS without Ca/ Mg, pH 7.2, Kantonsapotheke Zürich). Composites were cut into a rectangular form (length = 20 mm, width = 6 mm, thickness = 3 mm) with a blade and sterilized in ethylene oxide. The Young's modulus was measured using a tensile tester (Shimadzu AGS-X, 50 N load cell, Reinach, Switzerland). Samples were placed in the sample holder using pressurized air at 5 bar and stretched at a strain rate of 50 mm min^{-1}. An initial gauge length of 10 ± 1 mm was used. The Young's modulus was calculated at low strains of 0.05 in the linear regime of stress-strain curve using a tangent approximation. The sample sizes for the as prepared and implanted composites were $n = 5$ and $n = 4$, respectively.

2.4. *In ovo* characterization with a chick chorioallantoic membrane (CAM) assay

2.4.1. Sample preparation. Two different types of samples were prepared for the *in ovo* CAM assay. First, non-porous samples were cut to rectangular shapes (20 x 6 x 3 mm^3) with a scalpel in order to measure the mechanical properties after implantation. Second, porous samples were prepared by cutting the material to circular pieces with a diameter of 5 mm and a thickness of 3 mm using a scalpel for measurements of tissue biointegration. Once established that even much larger surface area non-porous samples had no tissue integration, comparisons between different porous samples were performed with smaller, more typically sized specimens for the CAM assay.[25]

Samples were washed in EtOH, gently wiped on paper and dried in vacuum overnight, subsequently. Sterilization was performed by ethylene oxide.

2.4.2. CAM assay: implantation of the composites onto the CAM. Fertilized Lohman white LSL chicken eggs were purchased from Animalco AG, Switzerland, and incubated at 37 °C and 65 % relative humidity in an incubator for 3.5 days. For experiments in chicken embryos until embryonic day 14 no IACUC approval is required according to Swiss animal care guidelines (TSchV, Art. 112). Afterwards, using a drill, a window was created in the eggshell after removing 2 mL of albumen. The window was covered with a Petri dish and incubated at 37 °C for another 3.5 days as described earlier.[26] On incubation day (ID) 7, the scaffolds were gently placed on top of the CAM, either without plastic ring for the nonporous samples (n = 8 for all groups) or with a plastic ring (diameter = 10 mm) for the porous samples (C: n = 5; mBG: n = 6; nBG: n = 11). Finally, the eggs were incubated for another 7 days, fixated in 4 % formalin solution in PBS, and incubated at 4 °C overnight. Then, the scaffolds were excised, embedded in paraffin, cross-sectioned into 5 μm slices and stained with hematoxylin/eosin (H&E).

2.4.3. Histological analysis. Integration factors for porous scaffolds were determined based on semi-quantitative scoring of H&E stained sections. Images were taken at 100x magnification using a light microscope (Leica DM 6000 B) equipped with a digital camera. In each histological section, five FOVs (Fields of View) were analysed, resulting in n = 15 for groups mBG and nBG and n = 30 for Control, respectively. The imprint of the scaffold on the CAM surface with its indentations was scored as a semi-quantitative tissue integration factor: 0 = no integration; 1 = slight integration; 2 = good integration and 3 = complete integration. Vascularization was assessed in the chorioallantoic membrane beneath each porous scaffold as well as 1 cm away from the material as a reference. It was semi-quantitatively scored: 0 = no vessels; 1

= very few vessels; 2 = few vessels; 3 = some vessels; 4 = a lot of vessels; 5 = highly vascularized (maximum) (for representative examples of each score, see Figure 5f).

The CAM thickness as well as the layer on top of the CAM (here referred to as collagen over layer) were measured below the scaffolds and 1 cm away in the same egg for comparison (here referred to as reference zone).

2.5. Statistical analysis

Results are given as mean ± standard deviation. Statistical significance was calculated using a one-way analysis of variance (ANOVA) with a Bonferroni's post-hoc correction (OriginPro 9.1.0, Origin Lab Corp. Northampton MA, USA). Statistical significance was assumed at a p value of $p < 0.05$.

3. Results

3.1. Particle characterization

Figure 1 shows the differences of BG micro- and nanoparticles. Microparticles had a shard-like appearance and a mean particle size of 4 μm as specified by the supplier. In contrast, nanoparticles had spherical shapes and an approximate primary particle size of 40-100 nm (see supporting information Figure S1). SEM analysis (Figure 1b and S1) revealed fusing of the flame-sprayed primary nanoparticles to larger agglomerates with an average agglomerate size of approximately 12 μm.[12, 21]

Analysis of the porogen (NH_4HCO_3) showed particles with an average primary particle size of 60 μm as seen in the particle size distribution of Figure 1d. NH_4HCO_3 contained particles of up to 400 μm in diameter. SEM images of the NH_4HCO_3 particles depicted non-spherical, non-agglomerated particles with different forms and softened edges.

3.2. Morphology of porous micro- and nanocomposites

The samples (micro- and nanocomposites) were highly porous with measured porosities in the range of 76 to 82 %. Pure silicone foam had a porosity of 81.6 ± 1.4% (n = 4), while the values for micro- and nanocomposites were 77.3 ± 1.4% (n = 4) and 75.6 ± 1.2% (n = 4), respectively. The samples had comparable pore sizes of up to 1 mm in diameter and were interconnected.

3.2.1. Thermogravimetric analysis. Thermogravimetric analysis revealed complete dissociation of NH_4HCO_3 under the manufacturing conditions of 200 °C for 2 hours without traces. Complete removal of the porogen from the silicone at the applied curing conditions were shown. Also, pure BG micro- and nanoparticles as well as pure silicone were not affected by the applied temperatures.

3.2.2. *In vitro* bioactivity study of porous samples. The bioactivity study in SBF showed the formation of HAp on and within the porous composites, incorporating BG. As seen in Figures 2e

and 2f, the HAp is formed evenly on the surface of the foams and within the pores. The presence of HAp after incubation in SBF was proven by its typical crystalline appearance in Figures 2h and 2i.[27] The presence of HAp was confirmed by FT-IR as for nano- and microcomposites, the characteristc band for CO_3^{2-} in carbonated apatites at 870 cm^{-1} was present.[28-29] The FT-IR spectrum of the nanocomposite also showed the characteristic double peak for the characteristic bending mode of the P-O-P bond in HAp at 570 cm^{-1} and 600 cm^{-1} (Figure S4).[29-30] The foaming procedure of silicone with NH_4HCO_3 did not have an effect on the bioactivity of the composites. Comparing the samples before (Figures 2a-2c) and after incubation in SBF (Figures 2d-2f) no changes of the general geometry of the pores were noted. The pore structure under simulated implanted conditions remained intact. Only the BG containing foam's surface structure seemed to be affected by the conditions in the SBF. The results of *%WL* and *%WA* are provided in the supporting information in Figure S2.

3.3. Mechanical properties

The stiffness of non-porous composites was affected by the modification with nBG particles. Incorporating solid nanoparticles resulted in significantly stiffer materials compared to pure silicone ($p < 0.05$), while microparticles did not increase the stiffness significantly compared to pure silicone ($p = 1$) (Figure 4). After implantation in chicken embryos the Young's modulus of pure silicone did not change compared to as prepared silicone ($p = 1$), while the ones of the micro- and nanocomposites changed significantly to its corresponding as prepared counterparts ($p < 7.8*10^{-4}$). Generally, incorporated BG particles stiffened silicone elastomers significantly *in ovo* compared to pure silicones ($p < 1.4*10^{-5}$).

3.4. *In ovo* CAM assay

Although different degrees of adhesion of the CAM were qualitatively distinguished for non-porous scaffolds, with increasing adhesion in the order of Control < mBG < nBG, semi-quantitative

scoring was only performed for porous scaffolds. During histological processing and cutting, materials were separated from the CAM surface. However, it was clearly found that the shape of the scaffold surface was reflected and similar to the shape of the CAM surface – the higher the integration the higher this similarity. Hence, scoring was performed and mBG and nBG were better integrated than pure silicone; with nBG even significantly better than mBG (Figure 5 c and d). Moreover, vascularization was semi-quantitatively scored beneath each porous scaffold. It was found that pure silicone evoked a significantly higher vessel density below the material as compared to the BG containing materials, for which mBG and nBG were not significantly different. In the reference zone, pure silicone evoked significantly higher vessel density than nBG.

In addition, CAM swelling was assessed by measuring the thickness (Figure S3a). The CAM was significantly thicker for BG containing materials compared to pure silicone, but not significantly different for mBG and nBG; the same was found for the collagen layer on top of the CAM (Figure S3b).

4. Discussion

We successfully showed that manipulating silicone by blending Bioglass 45S5® particles into silicone and forming a 3D-structure significantly improved tissue integration of the elastomer in an *in ovo* CAM assay. The simple manufacturing process of blending with BG particles and foaming with ammonium bicarbonate proved to be successful and reliable. Verified by HAp formation in an *in vitro* SBF assay we illustrated the bioactivity of the materials. A biomechanical analysis showed mechanical integrity of BG/silicone composites with expectable, but little stiffening under implanted *in ovo* conditions.

In order to address the adverse events of silicone implants, caused by the material's bioinertness, we decided to investigate the *in ovo* tissue biointegration of elastomeric silicone composites. The composites had been modified in their bulk by blending bioactive particles rather than modifying only the composites' surfaces. Ross *et al*. tackled the problem of insufficient tissue adhesion to peritoneal dialysis catheters by coating silicone tubing with melt-derived 45S5 Bioglass® particles. These particles were up to 125 μm in diameter, and the tubing was subcutaneously implanted in a rat model.[8] The BG coated sections were palpably fixed to the soft tissues as compared to the uncoated silicone, which did not show any adherence to the surrounding tissue.[8] In contrast to a coating, the goal of this study was to investigate, whether blending of BG particles into the material could have similar positive effects of tissue integration in silicone implants. Comparable attempts had been undertaken by Wang *et al*., however using rigid high density polyethylene (HDPE) rather than soft silicone rubber.[31] The authors blended Bioglass® microparticles (46 μm) into HDPE and could prove bioactivity in SBF, but did neither show an *in vitro* cell assay on the material nor any *in vivo* results.[31] In close similarity to the work of Wang *et al*., we decided to investigate the potential of blending bioactive micro- and nanoparticles into silicone in order to improve tissue adhesion of this type of soft, elastomeric and medically relevant implant material.

Manufacturing. The manufacturing process of blending BG45S5® particles into the elastomer prior to cross-linking was easy and versatile. We chose micro- and nanoparticles in order to compare the influence of the particle size, i.e. its surface area on the manufacturing process of the composites, its mechanical properties and its *in ovo* tissue integration. In contrast to Wang *et al*., who investigated particle volume fractions of up to 40 %, we limited the weight fraction of the bioactive particles to 5 wt% (2.14 vol%), because when using the same particles as previously reported it was shown that the maximum amount of nanoparticles to be incorporated into silicone elastomers is limited.[12, 31] This might be due to an incompatibility of silicone with BG, which is particularly enhanced for nanoparticles with a larger surface area as compared to microparticles with comparably small surface to volume ratios. Alternatively, also the nanoparticle-based inhibition of the platinum catalyst for the curing reaction of the silicone seems reasonable. This was reported earlier by Fahrni *et al*. for iron oxide nanoparticles in polydimethylsiloxane (PDMS).[32] The incorporation of larger amounts than 10 wt% nBG was not possible and already at this weight fraction, the mechanical integrity of the composites *in vitro* was significantly compromised.[12] Thus, we decided to limit our study to 5 wt% composite-loading.

The foaming procedure using ammonium bicarbonate in silicone elastomers was adapted from Lin *et al*. and Mac Murray *et al*..[33-34] NH_4HCO_3 was chosen, because it decomposes to the gaseous molecules ammonia, carbon dioxide and water above a temperature of approximately 60 °C (Figure 3). The gases formed the pores within silicone and were removed completely from the composite foams without residues.[34] A temperature of 200 °C was chosen, because we noted that for lower values, the porogen inhibited curing of the two-component silicone. This coincides with literature, which reports that NH_4HCO_3 inhibits the platinum catalyst in addition-cured PDMS resins.[34-35] We could overcome this problem by applying the comparably high temperature of 200 °C, which resulted in simultaneous curing of silicone and porogen removal. We did not apply

a pre-curing reaction at low temperatures before the removal of the porogen at elevated temperatures. In contrast to the production process of the porous samples, the elevated curing temberature of 200 °C was not required for the production of non-porous samples due to the absence of NH_4HCO_3. Thus, a lower temperature of 100 °C was chosen.

Composites. The foaming resulted in an open-pore structure, as already reported by Mac Murray *et al*., even though it is difficult to verify this with the SEM images presented in Figure 2.[34] However, we could show the interconnectivity of the pores by placing porous samples on absorbent paper and putting an EtOH drop on the samples. After a short period of time the absorbent paper was wetted by the EtOH, having passed through the porous sample. This verified the interconnectivity of the pores. Also, the presence of the BG particles did not seem to have a significant impact during the foaming of the composites, as the 3D-structure of all samples seemed to be comparable (Figure 2) as well as the porosity of approximately 80 % for each material.

The *in vitro* SBF assay proved the bioactivity of the porous and BG-containing composites, verified visually by HAp formation in the SEM images of the samples after incubation (Figure 2) and compared with previously published SEM images of HAp.[27] HAp formation was also validated by FTIR (Figure S4). The presence of HAp is crucial for the formation of a stable interface between the implant and soft tissue as it forms a bond to collagen fibrils.[14] Porous control samples without BG did not show any HAp, which verified the BG inflicted bioactivity of the composites. Also, it proved that using NH_4HCO_3 as porogen does not affect the bioactivity of the BG andthe composites. The presence of HAp, even deeper within the porous structure, could be verified. This served as a first approximation for possible tissue ingrowth into the 3D structure and, thus, as an approximation, whether a more stable 3D-fascilitated interface between the composite and the tissue can be achieved.

Mechanical properties. Incorporating BG into the non-porous elastomeric polymer resulted in a stiffening of the composites as compared to pure silicone (Figure 4), which coincides with theory and previous reports.[36] Rigid particles have larger moduli than silicone and when blended into the elastomer, increased the moduli thereof. The Young's modulus generally did not depend on particle/matrix interactions, because it was measured in the small strain regime, where no particle/matrix-debonding occurred.[36] Classical theories on the Young's modulus only give a dependency of the filler volume fraction and not filler diameter.[36-38] However, as also shown in our results, a larger Young's modulus was measured with a decreasing filler in primary particle size. This has been reported earlier in multiple studies and is being attributed to a critical particle size.[36] After implantation, the particle-loaded composites had significantly increased moduli, which had been reported earlier by us in an *in vitro* assay.[12] We attributed this to true reinforcement by nBG. Finer dispersion of the smaller nanoparticles formed crystalline and solid HAp across the bulk of the silicone *in vitro*, which increased the stiffening of the composites more than for mBG containing composites. HAp could only be formed very localized at the larger BG locations in microcomposites, thus not stiffening the material as much as in nanocomposites.[12, 39] We assume that this explanation also holds for a biomechanical *in vivo* assay.

CAM assay. The CAM assay is an easy and fast assay often used in the field of tissue engineering and regenerative medicine.[40]It allows short-term determination of a biomaterial's biocompatibility and integration into the chorioallantoic membrane of the chicken embryo.[41] First, we tested biointegration of non-porous silicone and composites during the 7-day incubation in the CAM assay. Although biointegration was weak for all the three materials tested, there was a qualitative difference between silicone and the composites during removing them from the CAM. While pure silicone rubber could easily be separated from the CAM surface by tweezers (tip width: 1 mm, approximate pulling force: 120 mN), because there was a visible gap between silicone and the

CAM, removal of mBG and nBG composites was more difficult, caused by the adhesion of the materials' flat surface to the membrane.

Secondly, we investigated the biointegration of porous silicone and composites. Confirming that pores support biocompatibility and biointegration of many biomaterials[42], we found that porous materials were better integrated compared to non-porous materials (data not shown). All materials (silicone, mBG and nBG) were not removable by using tweezers. Whilst overall integration remained poor in comparison to other materials, introduction of porosity significantly improved biointegration compared to the non-porous silicone and composites. After formalin fixation, the tissue-material construct was cut out as a whole and processed for histological analysis. Only during cutting with a microtome, the materials were separated from the CAM surface. However, the higher the tissue integration before cutting, the higher the similarity of the imprint on the CAM surface. Hence, we semi-quantitatively scored the integration (Figure 5). Obviously, pure silicone was less well integrated than the composites. The presence of BG, either micron-sized or nanosized, improved the quality of biointegration. When mBG was compared to nBG porous composites, there was even a better integration for the nanocomposites as compared to the microcomposites. Such findings stand in accordance with a study by Chan and coworkers where an inert polyetheretherketone (PEEK) was reinforced with HAp nanoparticles and compared to PEEK with HAp microparticles. They reported that nanocomposites showed not only improved mechanics but also an excellent biocompatibility and integration compared to the microcomposites.[43]

As for the vascularization of the CAM below the scaffolds, we found a higher vessel density for pure silicone as compared to the BG-containing materials which were both similarly vascularized. It might be speculated whether the bioglass or its transformation product hydroxyapatite decreased

the angiogenic response towards the BG/silicone scaffolds – the two components have been reported to act differently towards neovascularization.[44-45]

Limitations of the study. This study has several limitations. The CAM assay fulfills only gives information about the materials' short-term behavior in implanted conditions, meaning implantation for 7 days. It cannot predict the materials' properties, when it has to fulfill a certain function, in this case the formation of a stable silicone/skin interface to prevent infection. It gives important data on tissue adhesion and biocompatibility but only more complex animal studies will give certainty on the material capacity to fulfill a certain function.

5. Conclusion

The incorporation of BG45S5® into medical-grade silicone elastomer and forming a 3D-structure with a porogen significantly improves the tissue integration of the material *in ovo*. nBG/silicone composites have significantly improved biointegration compared to mBG/silicone composites. Either type of BG (micro or nano) improves the biointegration, compared to pure silicone. All BG-containing silicones show bioactivity also deeper within the pores. The pure incorporation of BG45S5®, irrespective of the particle size of the bioactive material and keeping a 2D geometry, does not yield stable tissue adhesion in a 7-day *in ovo* CAM assay. Whether a 2D material can form a more stable skin-silicone interface with improved healing in a possible application in percutaneous devices remains unknown, however is rather unlikely. The CAM assay showed the requirement for 3D porous structures to measure short-term improvements in tissue adhesion. The need for a 3D structure complicates the manufacturing procedure, especially when it has to be applied to a specific, existing implant with a required geometry. Still, it remains comparably easy. The mechanical properties prove stable materials within the measured time frame.

Summarizing, the manufacturing of the composites by simple blending of bioactive particles and forming a 3D structure in the clinically relevant material silicone is very easy, the *in ovo* results prove better tissue integration compared to pure silicone and the mechanical integrity remains intact.

Conflicts of interest

The authors declare no conflict of interest.

Acknowledgements

The authors gratefully acknowledge the financial support of the authors' institutions.

References

1. de Voogt, W. G., Pacemaker leads: performance and progress. *Am J Cardiol* **1999,** *83*, 187-191.
2. Zele, D. V.; Heymans, O., Breast Implants A Review. *Acta Chir Belg* **2004,** *104*, 158-165.
3. Merchel, R. A.; Reid, B. B.; McCandless, S. P.; Caine, W. T.; Ledford, I. D.; Clayson, S. E.; Carter, A. K.; Rasmusson, B.; Stoker, S.; Budge, D.; Alharethi, R. A.; Kfoury, A. G., Impact of Driveline Material and Size on Exit Site Healing Time in Left Ventricular Assist Devices. *J Heart Lung Transplant* **2012,** *31*, S21.
4. Cohrs, N. H.; Petrou, A.; Loepfe, M.; Yliruka, M.; Schumacher, C. M.; Kohll, A. X.; Starck, C. T.; Schmid Daners, M.; Meboldt, M.; Falk, V.; Stark, W. J., A Soft Total Artificial Heart - First Concept Evlauation on a Hybrid Mock Circulation. *Artif Organs* **2017,** *41*, 948-958.
5. Wilflingseder, P.; Propst, A.; Mikuz, G., Constrictive fibrosis following silicone implants in mammary augmentation. *Chir plast* **1974,** *2*, 215-229.
6. McCandless, S. P.; Ledford, I. D.; Mason, N. O.; Alharethi, R.; Rasmusson, B. Y.; Budge, D.; Stoker, S. L.; Clayson, S. E.; Doty, J. R.; Thomsen, G. E.; Caine, W. T.; Kfoury, A. G.; Reid, B. B.; Miller, D. V., Comparing velour versus silicone interfaces at the driveline exit site of HeartMate II devices: infection rates, histopathology, and ultrastructural aspects. *Cardiovasc Pathol* **2015,** *24*, 71-75.
7. Schoen, P., *Proceedings Medical Plastics*. Hexagon Holding ApS: Copenhagen, Denmark, 2002; Vol. 16.
8. Ross, E. A.; Batich, C. D.; Clapp, W. L.; Sallustio, J. E.; Lee, N. C., Tissue adhesion to bioactive glass-coated silicone tubing in a rat model of peritoneal dialysis catheters and catheter tunnels. *Kidney Int* **2003,** *63*, 702-708.
9. Williams, D. F., On the mechanisms of biocompatibility. *Biomaterials* **2008,** *29*, 2941-2953.
10. Isenhath, S. N.; Fukano, Y.; Usui, M. L.; Underwood, R. A.; Irvin, C. A.; Marshall, A. J.; Hauch, K. D.; Ratner, B. D.; Fleckman, P.; Olerud, J. E., A mouse model to evaluate the interface between skin and a percutaneous device. *J Biomed Mater Res* **2007,** *83*, 915-922.
11. Dean, D.; Kallel, F.; Ewald, G. A.; Tatooles, A.; Sheridan, B. C.; Brewer, R. J.; Caldeira, C.; Farrar, D. J.; Akhter, S. A., Reduction in driveline infection rates: Results from the HeartMate II Multicenter Driveline Silicone Skin Interface (SSI) Registry. *J Heart Lung Transplant* **2015,** *34*, 781-789.
12. Cohrs, N. H.; Schulz-Schönhagen, K.; Jenny, F.; Mohn, D.; Stark, W. J., Bioactive glass containing silicone composites for left ventricular assist device drivelines: role of Bioglass 45S5® particle size on mechanical properties and cytocompatibility. *J Mater Sci* **2017,** *52*, 9023-9038.
13. Hench, L. L., The story of Bioglass®. *J Mater Sci Mater Med* **2006,** *17*, 967-978.
14. Hench, L. L.; Splinter, R. J.; Allen, W. C.; Greenlee, T. K., Bonding mechanisms at the interface of ceramic prosthetic materials. *J Biomed Mater Res* **1971,** *5*, 117-141.
15. Hench, L. L., Bioceramics, a clinical success. *Am Ceram Soc Bull* **1998,** *77*, 67-74.
16. Miguez-Pacheco, V.; Hench, L. L.; Boccaccini, A. R., Bioactive glasses beyond bone and teeth: Emerging applications in contact with soft tissues. *Acta Biomater* **2015,** *13*, 1-15.
17. Gorustovich, A. A.; Roether, J. A.; Boccaccini, A. R., Effect of Bioactive Glasses on Angiogenesis: A Review of In Vitro and In Vivo Evidences. *Tissue Eng Part B Rev* **2009,** *16*, 199-207.

18. Lin, C.; Mao, C.; Zhang, J.; Li, Y.; Chen, X., Healing effect of bioactive glass ointment on full-thickness skin wounds. *Biomed Mater* **2012,** *7*, 045017.
19. Hu, S.; Chang, J.; Liu, M.; Ning, C., Study on antibacterial effect of 45S5 Bioglass®. *J Mater Sci Mater Med* **2009,** *20*, 281-286.
20. Jones, J. R.; Sepulveda, P.; Hench, L. L., Dose-dependent behavior of bioactive glass dissolution. *J Biomed Mater Res* **2001,** *58*, 720-726.
21. Brunner, T. J.; Grass, R. N.; Stark, W. J., Glass and bioglass nanopowders by flame synthesis. *Chem Commun* **2006,** *13*, 1384-1386.
22. Kokubo, T.; Takadama, H., How useful is SBF in predicting in vivo bone bioactivity? *Biomaterials* **2006,** *27*, 2907-2915.
23. Misra, S. K.; Ansari, T. I.; Valappil, S. P.; Mohn, D.; Philip, S. E.; Stark, W. J.; Roy, I.; Knowles, J. C.; Salih, V.; Boccaccini, A. R., Poly(3-hydroxybutyrate) multifunctional composite scaffolds for tissue engineering applications. *Biomaterials* **2010,** *31*, 2806-2815.
24. Kellenberger, C. R.; Pfleiderer, F. C.; Raso, R. A.; Burri, C. H.; Schumacher, C. M.; Grass, R. N.; Stark, W. J., Limestone nanoparticles as nanopore templates in polymer membranes: narrow pore size distribution and use as self-wetting dialysis membranes. *RSC Adv* **2014,** *4* (106), 61420-61426.
25. Woloszyk, A.; Liccardo, D.; Mitsiadis, T., Three-dimensional imaging of the developing vasculature within stem cell-seeded scaffolds cultured in ovo. *Front. Physiol.* **2016,** *7*.
26. Kivrak Pfiffner, F.; Waschkies, C.; Tian, Y.; Woloszyk, A.; Calcagni, M.; Giovanoli, P.; Rudin, M.; Buschmann, J., A New In Vivo Magnetic Resonance Imaging Method to Noninvasively Monitor and Quantify the Perfusion Capacity of Three-Dimensional Biomaterials Grown on the Chorioallantoic Membrane of Chick Embryos. *Tissue Eng Part C Methods* **2014,** *21*, 339-346.
27. Tas, A. C.; Bhaduri, S. B., Rapid coating of Ti6Al4V at room temperature with a calcium phosphate solution similar to 10× simulated body fluid. *J Mater Res* **2011,** *19* (9), 2742-2749.
28. S., K., Synthesis and characterization of hydroxyapatite crystals: A review study on the analytical methods. *J Biomed Mater Res* **2002,** *62* (4), 600-612.
29. Mačković, M.; Hoppe, A.; Detsch, R.; Mohn, D.; Stark, W. J.; Spiecker, E.; Boccaccini, A. R., Bioactive glass (type 45S5) nanoparticles: in vitro reactivity on nanoscale and biocompatibility. *J Nanopart Res* **2012,** *14*, 1-22.
30. Cerruti, M.; Greenspan, D.; Powers, K., Effect of pH and ionic strength on the reactivity of Bioglass® 45S5. *Biomaterials* **2005,** *26* (14), 1665-1674.
31. Wang, M.; Hench, L. L.; Bonfield, W., Bioglass®/high density polyethylene composite for soft tissue applications: Preparation and evaluation. *J Biomed Mater Res* **1998,** *42*, 577-586.
32. Fahrni, F.; Prins, M. W. J.; van Ijzendoorn, L. J., Magnetization and actuation of polymeric microstructures with magnetic nanoparticles for application in microfluidics. *J Magn Magn Mater* **2009,** *321*, 1843-1850.
33. Lin, H.-R.; Kuo, C.-J.; Yang, C. Y.; Shaw, S.-Y.; Wu, Y.-J., Preparation of macroporous biodegradable PLGA scaffolds for cell attachment with the use of mixed salts as porogen additives. *J Biomed Mater Res* **2002,** *63*, 271-279.
34. Mac Murray, B. C.; An, X.; Robinson, S. S.; van Meerbeek, I. M.; O'Brien, K. W.; Zhao, H.; Shepherd, R. F., Soft Robotics: Poroelastic Foams for Simple Fabrication of Complex Soft Robots. *Adv. Mater.* **2015,** *27*, 6334-6340.
35. de Buyl, F., Silicone sealants and structural adhesives. *Int J Adhes Adhes* **2001,** *21*, 411-422.

36. Fu, S.-Y.; Feng, X.-Q.; Lauke, B.; Mai, Y.-W., Effects of particle size, particle/matrix interface adhesion and particle loading on mechanical properties of particulate–polymer composites. *Compos Part B-Eng* **2008,** *39*, 933-961.
37. Einstein, A., Über die von der molekularkinetischen Theorie der Wärme geforderte Bewegung von in ruhenden Flüssigkeiten suspendierten Teilchen. *Ann Phys (Leipzig)* **1905,** *322*, 549-560.
38. Guth, E., Theory of Filler Reinforcement. *J Appl Phys* **1945,** *16*, 20-25.
39. Misra, S. K.; Mohn, D.; Brunner, T. J.; Stark, W. J.; Philip, S. E.; Roy, I.; Salih, V.; Knowles, J. C.; Boccaccini, A. R., Comparison of nanoscale and microscale bioactive glass on the properties of P(3HB)/Bioglass® composites. *Biomaterials* **2008,** *29*, 1750-1761.
40. Moreno-Jiménez, I.; Kanczler, J. M.; Hulsart-Billstrom, G.; Inglis, S.; Oreffo, R. O. C., The Chorioallantoic Membrane Assay for Biomaterial Testing in Tissue Engineering: A Short-Term In Vivo Preclinical Model. *Tissue Eng Part C Methods* **2017,** *23*, 938-952.
41. Tomco, M.; Petrovova, E.; Giretova, M.; Almasiova, V.; Holovska, K.; Cigankova, V.; Jenca, A.; Jencova, J.; Jenca, A.; Boldizar, M.; Balazs, K.; Medvecky, L., In vitro and in vivo study of microporous ceramics using MC3T3 cells, CAM assay and a pig animal model. *Anat Sci Int* **2017,** *92*, 569-580.
42. Ratner, B. D., A pore way to heal and regenerate: 21st century thinking on biocompatibility. *Regen Biomater* **2016,** *3*, 107-110.
43. Chan, K. W.; Liao, C. Z.; Wong, H. M.; Kwok Yeung, K. W.; Tjong, S. C., Preparation of polyetheretherketone composites with nanohydroxyapatite rods and carbon nanofibers having high strength, good biocompatibility and excellent thermal stability. *RSC Adv* **2016,** *6*, 19417-19429.
44. Camilo, C. C.; Silveira, C. A. E.; Faeda, R. S.; Rollo, J.; Purquerio, B. D.; Fortulan, C. A., Bone response to porous alumina implants coated with bioactive materials, observed using different characterization techniques. *Journal of Applied Biomaterials & Functional Materials* **2017,** *15* (3), E223-E235.
45. Janko, M.; Sahm, J.; Schaible, A.; Brune, J. C.; Bellen, M.; Schroder, K.; Seebach, C.; Marzi, I.; Henrich, D., Comparison of three different types of scaffolds preseeded with human bone marrow mononuclear cells on the bone healing in a femoral critical size defect model of the athymic rat. *J. Tissue Eng. Regen. Med.* **2018,** *12* (3), 653-666.

Figure legends

Figure 1. Scanning electron microscopy (SEM) images of Bioglass 45S5® microparticles (a) and nanoparticles (b). (c) and (d) depict the SEM image and the particle size distribution of ammonium bicarbonate, respectively.

Figure 2. Scanning electron microscopy (SEM) images of Bioglass®/silicone composites before and after incubation in simulated body fluid (SBF) for 4 weeks. (a), (b) and (c) show pure silicone foam, silicone incorporating 5 wt% micron sized Bioglass® (BG) and silicon incorporating BG nanoparticles (5 wt%) as prepared, while (d), (e) and (f) show the respective samples after incubation in SBF. (g), (h) and (i) are close-up images of the samples after incubation in SBF and show the structure of hydroxyapatite in the case of microcomposites (h) and nanocomposites (i).

Figure 3. Thermogravimetric analysis of the manufacturing process.

Figure 4. Influence of *in ovo* environment in chicken embryos in a chick chorioallantoic membrane (CAM) assay on the mechanical properties of non-porous Bioglass 45S5®/silicone elastomer composites. (a) gives the stress-strain curve in the small strain region and (b) gives the Young's modulus of the materials as prepared ($n = 5$) and after implantation in chicken embryos for 7 days (post *in ovo*, $n = 4$). (control: pure silicone elastomer; mBG: silicone elastomer with 5 wt% Bioglass® (BG) microparticles; nBG: silicone elastomer with 5 wt% BG nanoparticles; *: significant differences for $p < 0.05$)

Figure 5. Results and analysis of the *in ovo* chick chorioallantoic membrane (CAM) assay of porous and non-porous Bioglass 45S5®/silicone elastomer composites. (a) shows the samples on

the CAM (left: non-porous, right: porous). (b) exemplifies imprints left behind by the scaffolds on the CAM. (c) shows the measured integration factor in porous composites with weight concentrations of 5 wt% microparticles (mBG) and 5 wt% nanoparticles (nBG). (d) defines the integration factor based on histological cuts of the tissue (for control and mBG: n = 15 FOVs; for nBG: n = 30 FOVs). The scores are defined as: 0 = no integration; 1 = slight integration; 2 = good integration and 3 = complete integration. (e) shows the semi-quantitatively determined vascularization extent below the scaffods in the chorioallantoik membrane with 0 = no vessels; 1 = very few vessels; 2 = few vessels; 3 = some vessels; 4 = a lot of vessels; 5 = highly vascularized (*: significant differences for $p < 0.05$; ***: significant differences for $p < 0.0001$), and (f) defines the vascularization scores by representative histological sections.

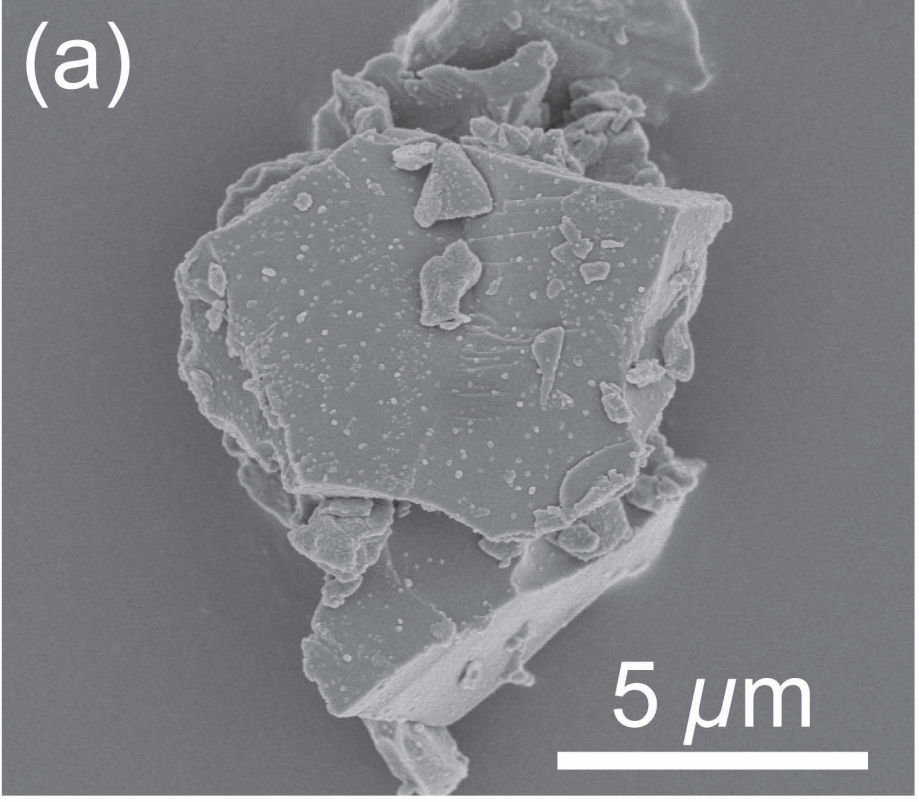
(a)
5 μm

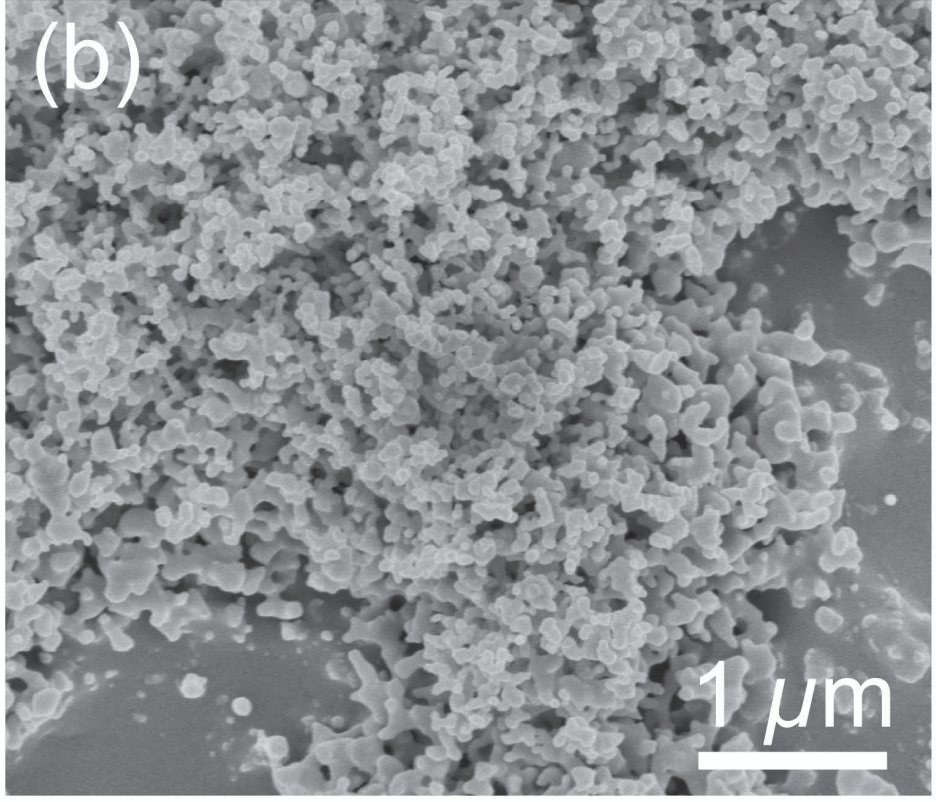
(b)
1 μm

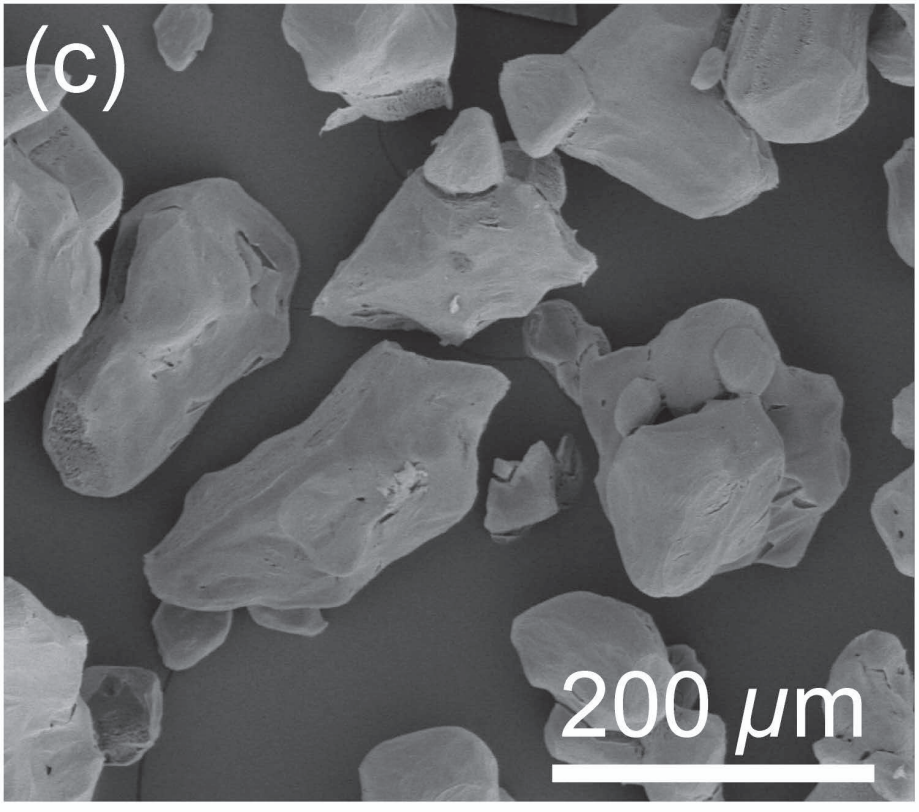
(c)
200 μm

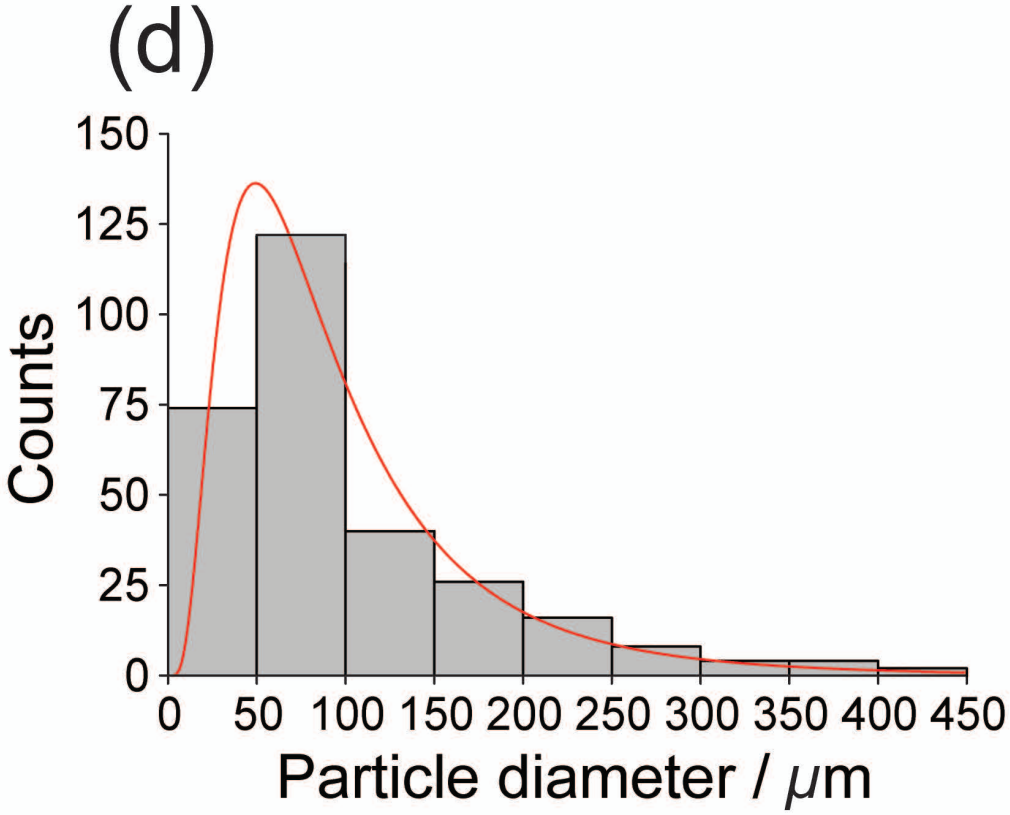
(d)
Counts
150
125
100
75
50
25
0
0 50 100 150 200 250 300 350 400 450
Particle diameter / μm

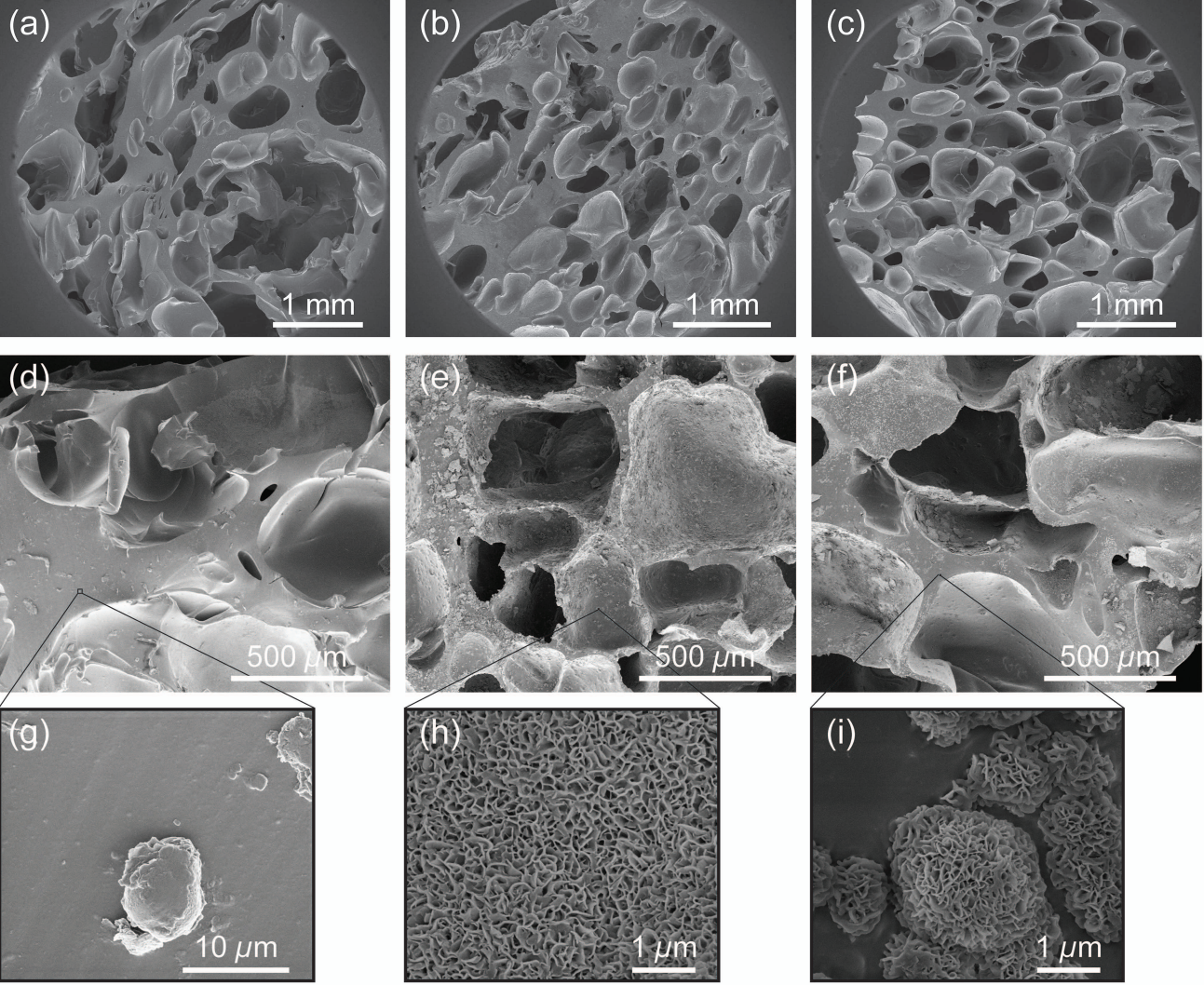
(a)
1 mm
(b)
1 mm
(c)
1 mm
(d)
500 μm
(e)
500 μm
(f)
500 μm
(g)
10 μm
(h)
1 μm
(i)
1 μm

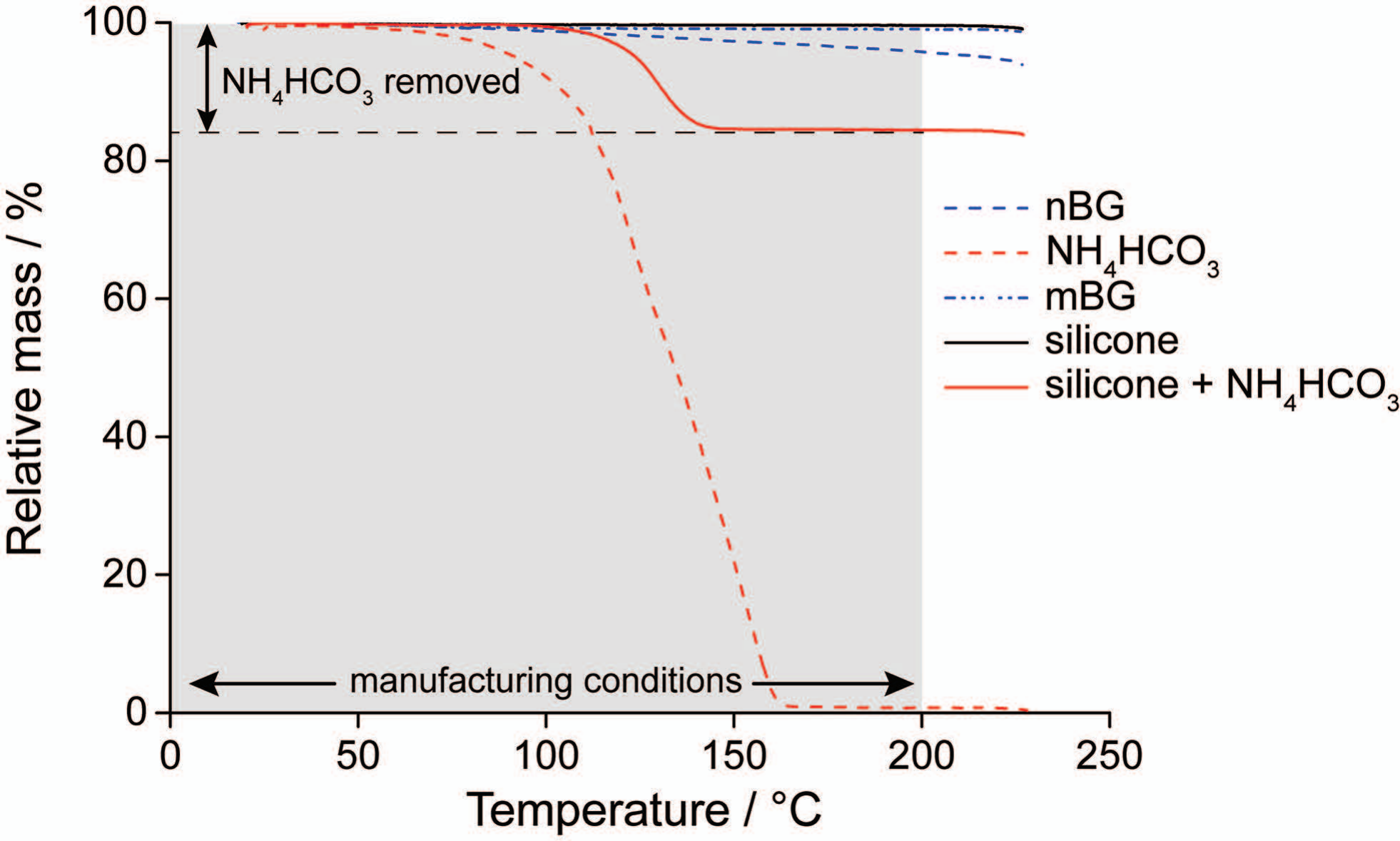
100
80
60
40
20
0
Relative mass / %
NH4HCO3 removed
manufacturing conditions
0
50
100
150
200
250
Temperature / °C
nBG
NH4HCO3
mBG
silicone
silicone + NH4HCO3

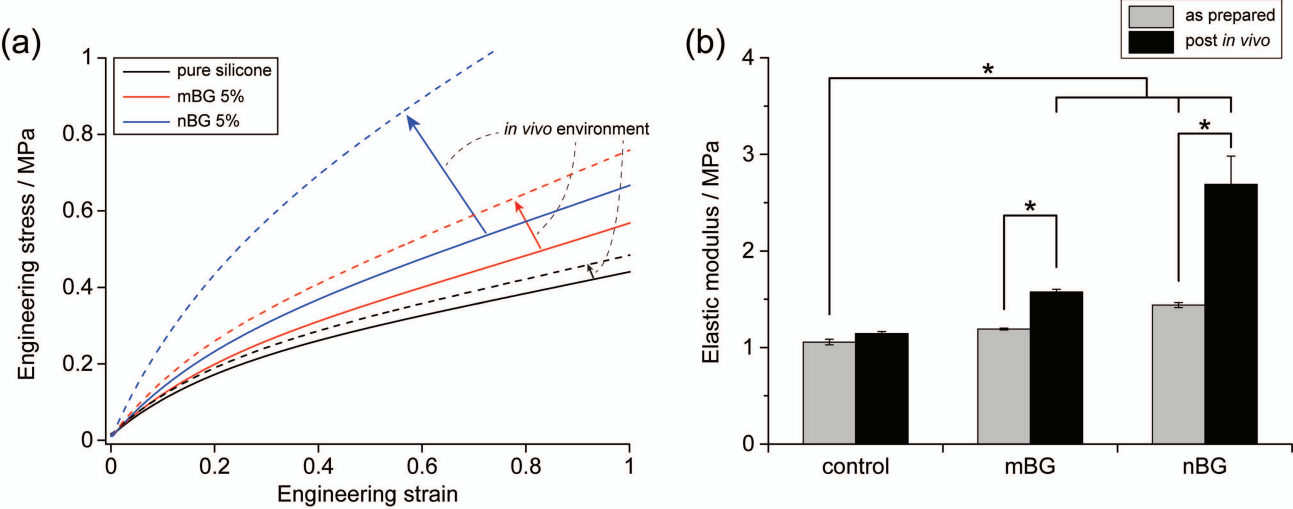
(a)
pure silicone
mBG 5%
nBG 5%
in vivo environment
Engineering stress / MPa
Engineering strain
0
0.2
0.4
0.6
0.8
1
(b)
as prepared
post in vivo
Elastic modulus / MPa
0
1
2
3
4
*
*
*
control
mBG
nBG

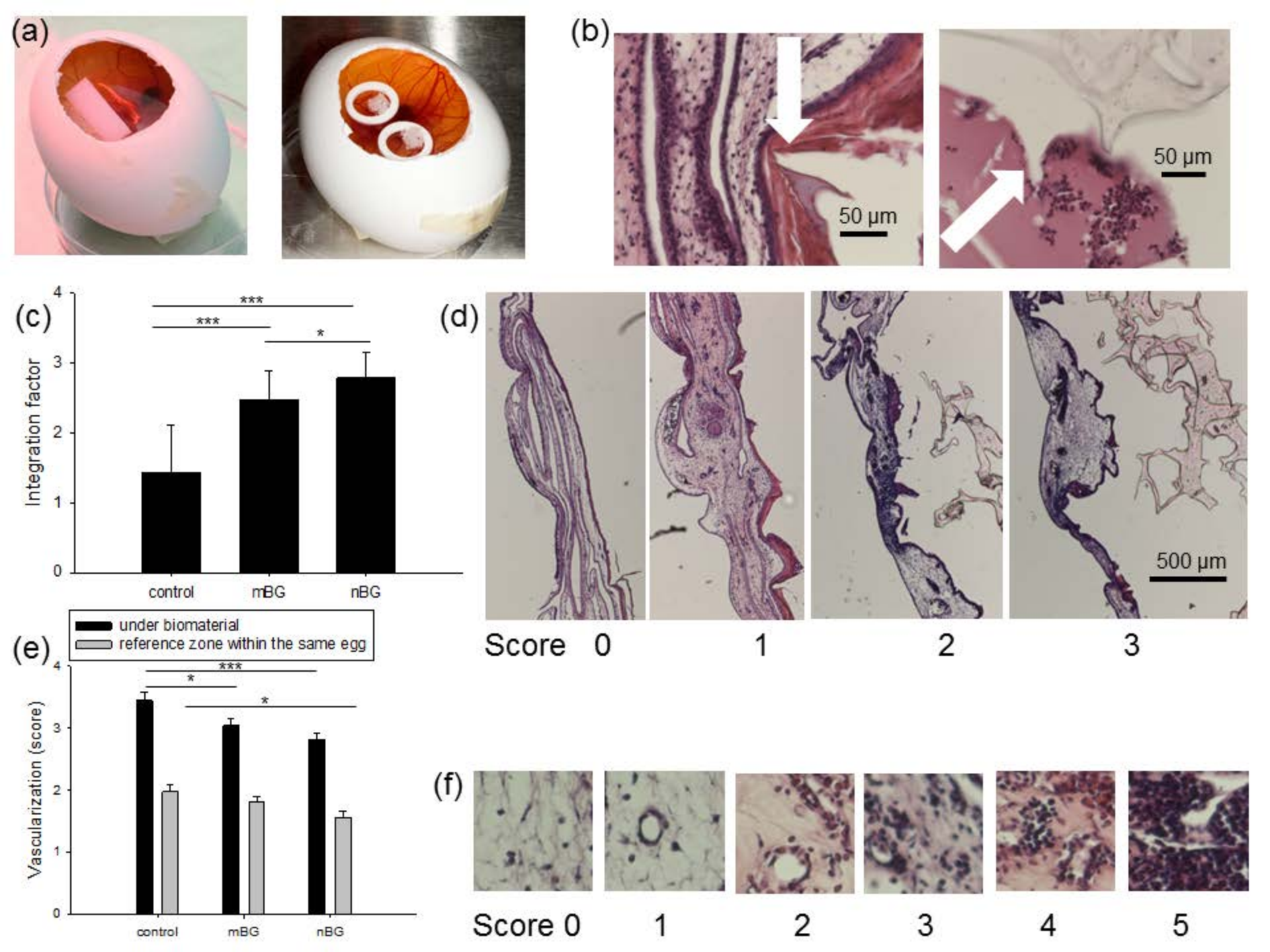
(a)
(b)
50 µm
50 µm
(c)
Integration factor
***
***
*
control
mBG
nBG
(d)
500 µm
Score 0
1
2
3
(e)
under biomaterial
reference zone within the same egg
Vascularization (score)
***
*
*
control
mBG
nBG
(f)
Score 0
1
2
3
4
5

Supporting Information

Journal of Biomedical Materials Research Part B – Applied Biomaterials

Modification of silicone elastomers with Bioglass 45S5® increases *in vivo* tissue biointegration

Nicholas H. Cohrs[1], Konstantin Schulz-Schönhagen[1], Dirk Mohn[1, 2], Petra Wolint[3], Gabriella Meier Bürgisser[3], Wendelin J. Stark[1] and Johanna Buschmann[3, *]

[1] Institute for Chemical- and Bioengineering, Department of Chemistry and Applied Biosciences, ETH Zürich, Zürich, Switzerland
[2] Clinic of Preventive Dentistry, Periodontology and Cariology, University of Zürich, Center of Dental Medicine, Zürich, Switzerland
[3] Division of Plastic and Hand Surgery, University Hospital Zürich, ZKF, Zürich, Switzerland

Emails:

NHC: nicholas.cohrs@chem.ethz.ch
KSS: konstantin.schulz-schoenhagen@chem.ethz.ch
DM: dirk.mohn@chem.ethz.ch
PW: Petra.Wolint@usz.ch
GMB: Gabriella.MeierBuergisser@usz.ch
WJS: wstark@ethz.ch
JB: johanna.buschmann@usz.ch

Corresponding Author

* Dr Johanna Buschmann, University Hospital Zürich, Division of Plastic and Hand Surgery, E LAB 27, Sternwartstrasse 14, 8091 Zürich, Switzerland. johanna.buschmann@usz.ch, Phone: +41 44 255 98 95, Fax: +41 44 255 50 47

1. Scanning election microscopy images

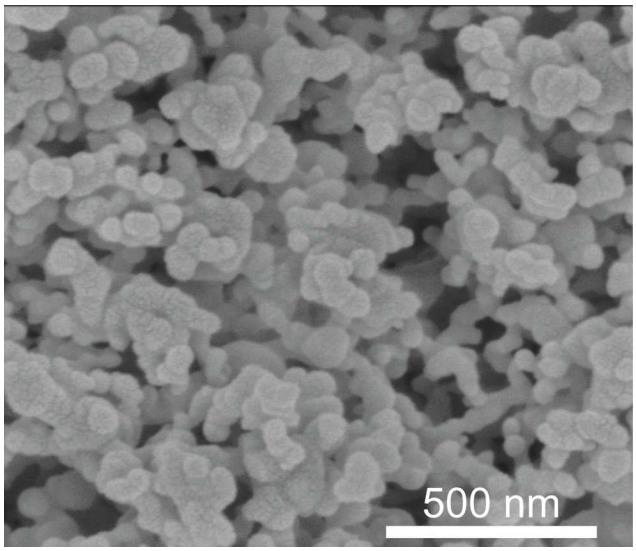

Figure S1. Scanning election microscopy image of nanosized Bioglass 45S5® particles.

2. Weight loss and water uptake of samples

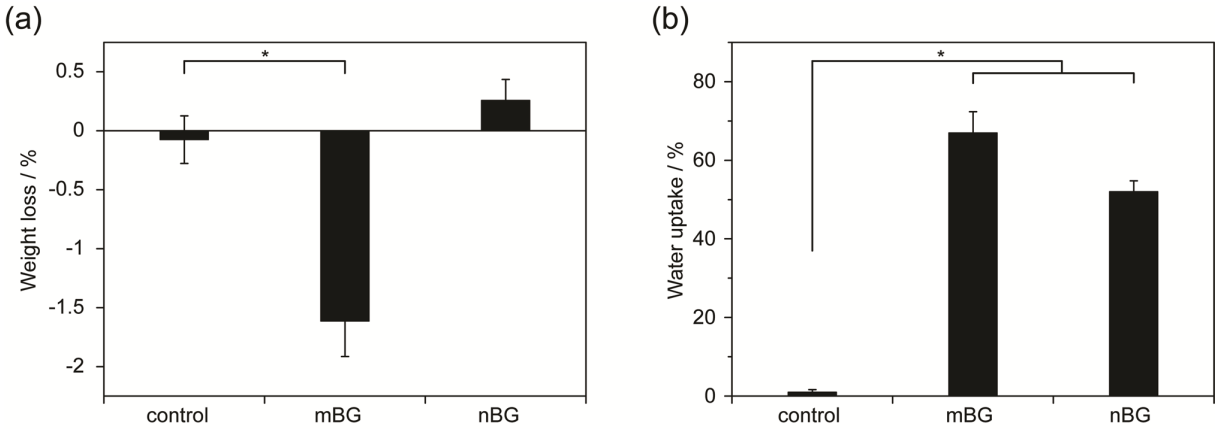

Figure S2. Depiction of the weight loss (a) and water uptake (b) of the porous pure silicone (control), porous silicone, containing 5 wt% Bioglass 45S5® microparticles (mBG) and porous silicone, containing 5 wt% Bioglass 45S5® nanoparticles (nBG). (*: significant differences for $p < 0.05$)

3. CAM thickness and collagen over layer

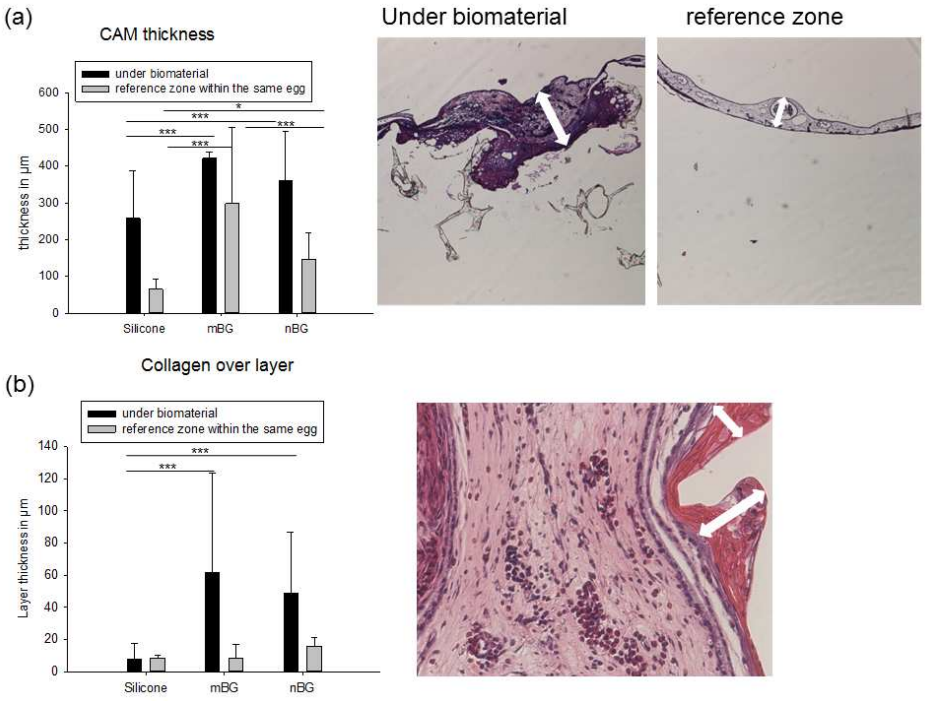

Figure S3. CAM thickness below the porous scaffolds and 1 cm away from the scaffolds (reference zone) (a) and collagen over layer as a response towards the on-planted scaffolds (b). (*: significant differences for $p < 0.05$; ***: significant differences for $p < 0.0001$)

4. FT-IR assessment

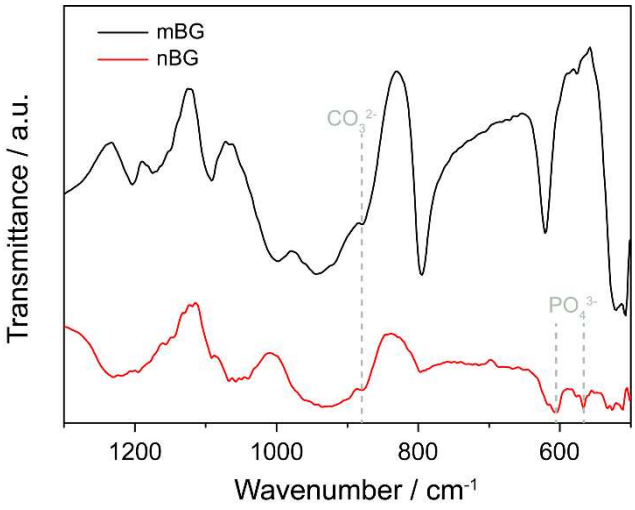

5.

Figure S4. FTIR spectra of nano- and microcomposites after immersion in simulated body fluid (SBF) for four weeks. As background the respective materials before immersion in SBF were used. Both composites show the characteristic peak of the CO_3^{2-} group in carbonated apatite, which serves as the proof for hydroxyapatite formation.